Arraycount, an algorithm for automatic cell counting in microwell arrays

Nezamoddin N. Kachouie[1,2], Lifeng Kang[1,2,3], and Ali Khademhosseini[1,2]
[1]Center for Biomedical Engineering, Department of Medicine, Brigham and Women's Hospital, Harvard Medical School, Cambridge, MA, USA, [2]Harvard-MIT Division of Health Sciences and Technology, Massachusetts Institute of Technology, Cambridge, MA, USA, and [3]Department of Pharmacy, National University of Singapore, Singapore

Microscale technologies have emerged as a powerful tool for studying and manipulating biological systems and miniaturizing experiments. However, the lack of software complementing these techniques has made it difficult to apply them for many high-throughput experiments. This work establishes Arraycount, an approach to automatically count cells in microwell arrays. The procedure consists of fluorescent microscope imaging of cells that are seeded in microwells of a microarray system and then analyzing images via computer to recognize the array and count cells inside each microwell. To start counting, green and red fluorescent images (representing live and dead cells respectively), are extracted from the original image and processed separately. A template-matching algorithm, is proposed in which pre-defined well and cell templates are matched against the red and green images to locate microwells and cells. Subsequently, local maxima in the correlation maps is determined and local maxima maps are thresholded [Q1]. At the end, the software records the cell counts for each detected microwell on the original image in high-throughput. The automated counting was shown to be accurate compared with manual counting, with a difference of ~1–2 cells per microwell: based on cell concentration, the absolute difference between manual and automatic counting measurements was 2.5–13%.

Introduction

Recently, microscale technologies have emerged as a powerful tool for high-throughput cellular and biological studies by enabling miniaturized experiments (1–3). These miniaturized well arrays can be used to segregate cells for single-cell analysis (4–6) and multiple-cell studies, such as to form neurospheres and embryoid bodies (7,8). Typically, these arrays contain hundreds or thousands of microwells, such that the throughput is significantly higher than those conducted using traditional multi-well plates. For example, a hydrogel microwell array was used to clonally [Q2] analyze neural stem cell (NSC) fates to demonstrate that neurosphere formation can be attributed to a single cell. Using time-lapse microscopy and immunostaining, the fate of several hundred single NSCs was tracked simultaneously (9).

The increase in the number of high-throughput cellular and biological studies have generated a need for high-throughput analysis and screening tools capable of processing the raw data and presenting it in a meaningful and efficient way. New advancement in digital imaging has made it possible to image biological events on micro- and nanoscale levels. To solve combinatorial problems related to cell biology and medical science, such as optimization of materials or screening of chemical libraries, images are taken from systems such as microwell arrays in which a large number of experiments are investigated in parallel. High-throughput image processing techniques are desired in order to analyze such images, but image processing and pattern recognition techniques are not adequately developed to analyze such biological and medical images. To investigate large numbers of images and to address new questions in biological and medical research, further design and development of digital cytometry techniques is required.

An important problem in many high-throughput experiments—specifically in stem cell engineering and drug discovery—is the analysis of cell viability in thousands of parallel experiments spotted in micro- and nanoliter volumes. To quantify cell viability in microwells, the number of cells in each microwell of a microarray system must be counted. Manual cell counting as a practical approach has been widely used; however, these results may be subjective and vary from person to person. Moreover, this is a tedious and laborious task that is prone to error due to the large number of measurement and analysis steps. Therefore, advanced techniques in digital image processing and pattern recognition must be employed for emerging biological applications.

Cell recognition and counting in microwell systems is an attractive and challenging task due to the presence of debris, high noise, and the difficulties of adapting available image segmentation approaches. It is imperative that cells in these substrates be imaged and automatically analyzed in a high-throughput manner. A variety of semi-automatic or automatic methods have been proposed for applications of image processing techniques to medical and biomedical research (10–13). However, the lack of software complementing such techniques makes it difficult for high-throughput screening. Currently available software—or example, imageJ (http://rsbweb.nih.gov/ij), and Cellprofiler (www.cellprofiler.com)—can only count the total number of cells in a defined region, which is not suitable for analyzing microwell array cell data in large quantities. Cellprofiler provides 'Grid Analysis' emulating hema-cytometer format, but it is limited to grid annotation or cell colony intensity measurement (14). For imageJ, the region of interest could be defined by using macros to segregate individual spots but this may not be suitable to process many images in high-throughput. Proprietary microarray software, such as Quantarray (Packard BioChip Technologies, Billerica, MA, USA) [Q3]and Genepix (Molecular Devices, Sunnyvale, CA, USA), while allowing user to define individual arrays
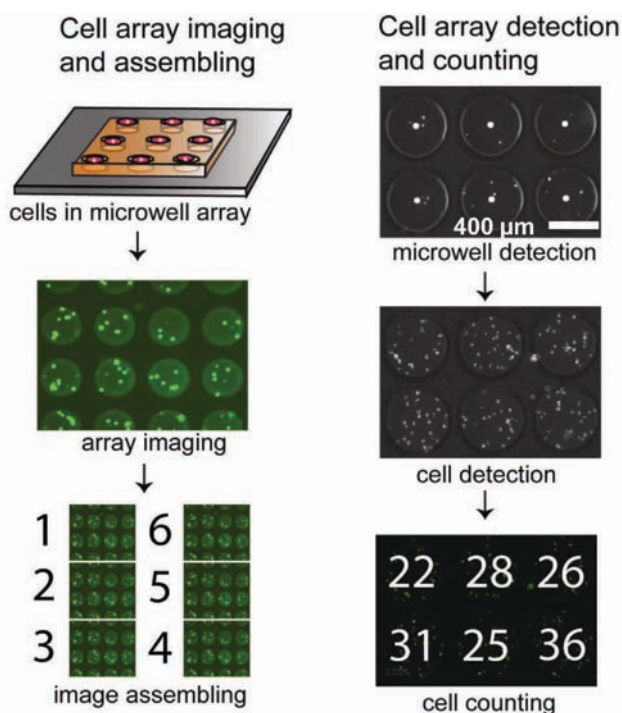
Figure 1. Schematic representation of the imaging and counting processes. The imaging process (left) includes imaging the microarray and stitching separate images together to form the whole field of the entire microarray. The proposed counting method (right) localizes the microwells in order to localize and count cells inside each microwell **[Q14]**.

on one image, cannot recognize the arrays automatically. Moreover, the readout from such microarray software is generally limited to fluorescent intensity and gives no direct cell counting. MetaMorph (Molecular Devices) has a wide range of application modules with intuitive setting selections for biology analysis. The software has an application module for Count Nuclei but it seems it does not give the number of cells in individual spots in a microarray system in a high-throughput manner. Cellomics is a complete system for high-content screening (HCS) and high-content analysis (HCA) (Pittsburgh, PA, USA). The Thermo Scientific Cellomics is a powerful platform including automated imaging, image analysis software, and high-content informatics which is coupled with reagents, and laboratory automation. As a total platform, it is equipped with hardware and software to perform both imaging and image analysis. It seems that in order to use the software, the user needs the entire platform. This software has an application named "Spot Detector" to count receptors, nuclei, and cells, but it does not appear to give the number of cells in each microwell in high-throughput. Most software is focused on overall cell or cell colony counting. For example ScanCount and CHiTA can only give the number of cell colonies automatically, but not the individual cell numbers in the culture plate (15,16). Although many

studies of bioimage informatics have been done over the past few years, software for cell counting in microarray format still remains largely underdeveloped (17).

The goal of this study was to develop an algorithm (i.e., ArrayCount) to analyze cell microarray images by automatically detecting a microwell array and then counting viable cells in each microwell. To do this, we stained the cells with fluorescent viability dyes, seeded cells in microwells, and then imaged the resulting arrays by fluorescence microscopy. The images were then loaded into the software for automatic cell counting (Figure 1).

Materials and methods
Materials
3-(Trimethoxysilyl)propyl methacrylate (TMSPMA), 2-hydroxy-2-methyl propiophenone, polyethylene glycol diacrylate (PEGDA), were purchased from Sigma-Aldrich (St. Louis, MO, USA). A live/dead staining kit [calcein AM and ethidium homodimer 1 (EthD-1) **[Q4]**] was purchased from Invitrogen (Carlsbad, CA, USA). Pluripotent murine embryonic stem (ES) cells, R1 strain, were obtained from the Mount Sinai Hospital in Toronto, Canada. Pre-cleaned microscope glass slides were purchased from Fisher Scientific (Waltham, MA, USA). Mouse leukemia inhibitory factor (LIF),

ESGRO was purchased from Chemikon Int. Inc., (Eugene, OR, USA). All other tissue culture components were purchased from Invitrogen. All chemicals were used as supplied without further purification.

Microwell fabrication
A detailed procedure of a microwell fabrication process has been reported earlier (18). In summary, a photolithographic approach was used in which a UV-photo-crosslinkable polyethylene glycol diacrylate (PEGDA;MW = 258) solution containing 0.5% (w/w) of the photoinitiator 2-hydroxy-2-methyl propiophenone was placed on a TMSPMA treated glass slide. The precursor solution was placed between a coated glass slide and a piece of cover glass with a photomask on top. Microscopy coverslips were used as spacers between the glass support and the cover glass to define the depth of the microwells. The precursor solution was then irradiated through a bright field photomask with UV light. The precursor solution did not undergo radical polymerization in the areas shaded by the photomask and remained water soluble. After curing the polymers, the cover glass was carefully removed and the microwells were developed by removing the uncrosslinked macromer with deionized water. The final microwell arrays contained 400 and 1089 microwells in 20 × 20 and 33 × 33 array formats with center-to-center spacings of 500 μm and 300 μm, respectively. All microwells were 150 μm deep.

Manual cell counting
Prior to seeding, cells were stained with the live/dead stain kit. Live cells were stained with calcein AM **[Q5]**, a polyanionic dye that is well retained in live cells, and which produces an intense, uniform green fluorescence [exitation/emission (ex/em): ~495 nm (blue)/~515 nm (green)]. Dead cells were stained with EthD-1, which enters the damaged cell membranes, undergoes a 40-fold enhancement of fluorescence upon binding to nucleic acids, and produces a bright red fluorescence [ex/em: ~495 nm (green)/~635 nm (red)]. PEG microwells were visible with poor contrast in the red image. The reason is because of the adsorption of cationic dyes on PEG, which might be because of solubilization or entrapment by the protruding oxy-ethylene groups on the surface (19). Concentrations of 2 μM and 4 μM were used for the calcein AM and EthD-1, respectively. Cells were pelleted and suspended in 1 mL of the staining solution for 10 min in an incubator. The cells were then re-pelleted and re-suspended in media and seeded in the wells as reported earlier (18). Six sets
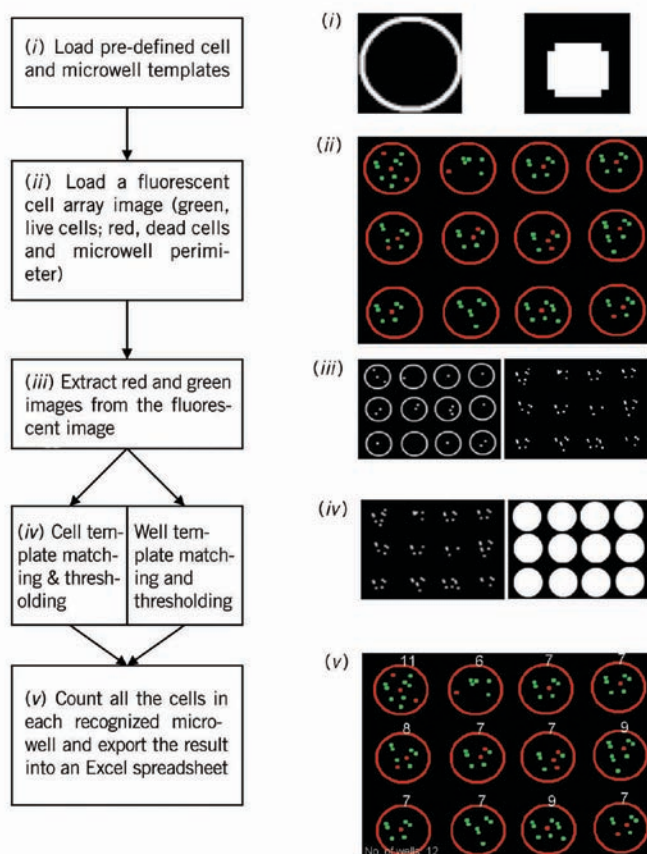
Figure 2. Process flow-diagram of the software. A color fluorescent image is decomposed to red, green, and blue images. Then predefined cell and well templates were matched against the green and red images to locate cells and wells. Afterward, the local maxima in the correlation maps were located and thresholded.

of images were taken manually with 2× magnifications for each microwell after cell seeding **[Q6]**. Each image set was composed of a green image and a red image which were taken using a fluorescent microscope at two wavelengths corresponding to the live and dead staining dyes, respectively, and were superimposed for cell counting. The number of cells were counted manually using ImageJ.

Software cell counting

Software cell counting operates by automatically locating individual or aggregates of cells as well as the microwells. Locating wells and cells is essentially an inverse problem, which can be addressed as a deconvolution problem. To solve the problem, we developed a method to effectively locate wells and detect individual cells.

To image a microarray after live/dead cell staining, six fluorescent images were taken in 3 × 2 mosaic format and stitched together. C was defined to be a fluorescent image which can be decomposed to red R, green G, and blue B images. In our analysis, G was used for live cell detection while R

was used for both dead cell localization and well detection (Figure 2).

The proposed method is based on matching a user-defined template by sliding it over the image pixel by pixel to find the objects in the image that are most similar to the template [well and cell synthetic templates are shown in Figure 2, part (*i*)]. To do this, the color fluorescent image is decomposed to red and green images as is shown in Figure 2, part (*iii*). As it can be seen, microwells and dead cells were visible in red image while live cells emerged in the green image. To detect microwells, the user-defined well template [Figure 2, part (*i*), left] is matched to the red image [Figure 2, part (*iii*), left]. A well correlation map is generated by sliding the well template over the image pixel by pixel and computing the correlation. The brighter pixels in the well correlation map [Figure 2, part (*iv*), left], represent the microwell centers.

In the same way, the cell template depicted in Figure 2 [part (*i*), right] was matched against the green and red images [Figure 2, part (*iii*)] to detect live and dead cells, respectively. After localizing the microwells and detecting live and dead

cells, the number of live and dead cells that were encircled in each microwell was counted and recorded [Figure 2, part (v)].

Cell Localization

Cell localization consists of cell template generation, template matching, cell center localization, and cell counting. As depicted in Figure 2, live cell localization, dead cell localization, and well detection can be processed in parallel. Here we propose a general approach whereby a user may generate a specific cell template based on the data set. Given that G is a green image (from 3 × 2 mosaic images) defined on a fixed digital grid, D:

$$G = \{G_{ij} \,|\, (i, j) \in D\}$$

[Eq. 1]

and z_{lc} is the set of live cell centers in green image consisting of q_{lc} live cell centers:

$$z_{lc} = \left\{z_{lc}^{k} \,\middle|\, k \in [1, q_{lc}]\right\}$$

[Eq. 2]

a disk shape template h_c is defined to represent a live/dead cell. The cell template is then convolved with the green image G to generate a correlation map for live cells:

$$H_{lc} = G * h_c$$

[Eq. 3]

The live cell correlation map obtained by applying the cell template to the green image is depicted in Figure 3A, part (*i*) **[Q7]**. The brighter pixels in the correlation map show the highly correlated points which are more likely to be cell centers. To locate the cell centers and remove the unlikely ones, we found the local maxima in the correlation map:

$$L_{lc} = l\left(H_{lc}, W_{lc}\right)$$

[Eq. 4]

where l is a function to locate the local maxima, L_{lc} is located local maxima in image G, and W_{lc} is the window size to be locally searched for the local maxima. The cell center map as depicted in Figure 3A, part (*ii*) is generated by thresholding the local maxima map:
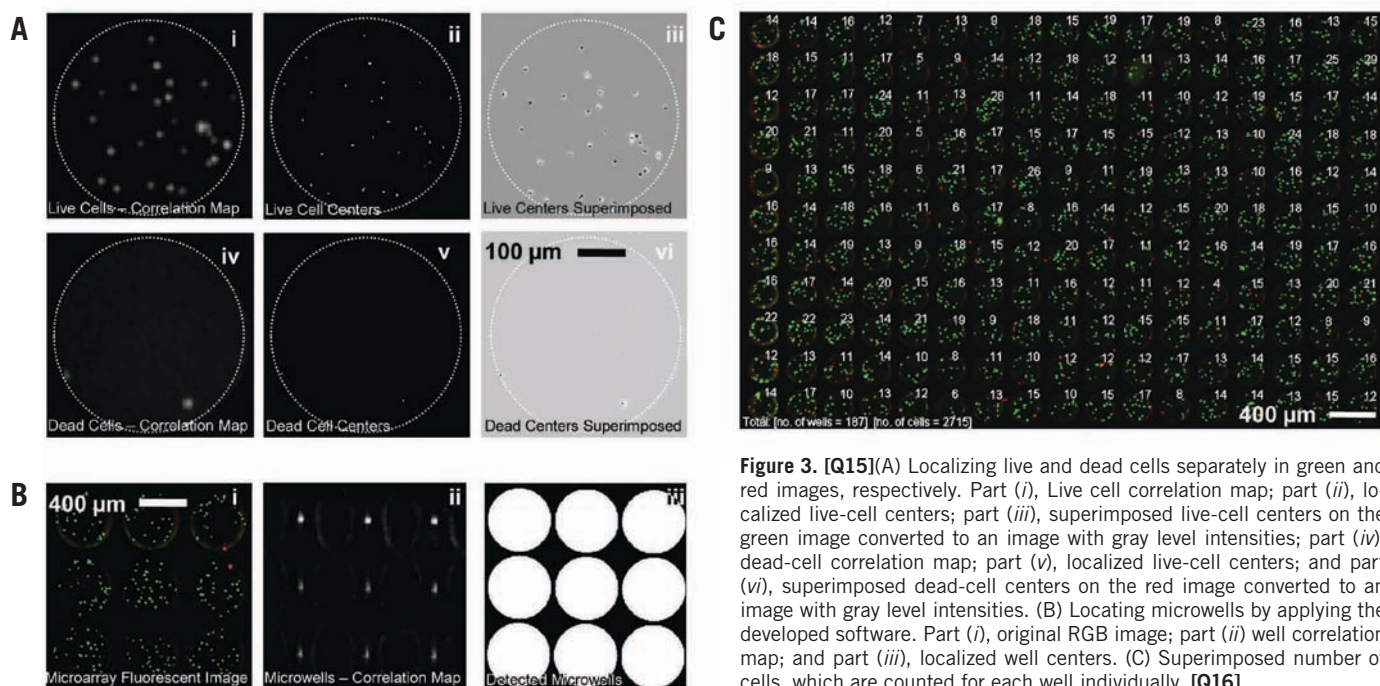
Figure 3. [Q15](A) Localizing live and dead cells separately in green and red images, respectively. Part (*i*), Live cell correlation map; part (*ii*), localized live-cell centers; part (*iii*), superimposed live-cell centers on the green image converted to an image with gray level intensities; part (*iv*), dead-cell correlation map; part (*v*), localized live-cell centers; and part (*vi*), superimposed dead-cell centers on the red image converted to an image with gray level intensities. (B) Locating microwells by applying the developed software. Part (*i*), original RGB image; part (*ii*), well correlation map; and part (*iii*), localized well centers. (C) Superimposed number of cells, which are counted for each well individually. **[Q16]**

$$Z_{lc} = T\left(L_{lc}, \tau_{lc}\right)$$

$$[\text{Eq. 5}]$$

where T is a thresholding function to return a thresholded set Z_{lc} containing those local maxima whose values are greater than the threshold value τ_{lc}. The threshold value τ_{lc} is set by minimizing the number of misdetections and false alarms.

In the same way that live cells were localized, dead cells were localized using red image R. The dead cell correlation map which was obtained by applying the cell template is depicted in Figure 3A, part (*iv*). The dead cell center map as depicted in Figure 3A, part (*v*) was finally generated by theresholding the dead cell local maxima map.

Well Detection

We took advantage of the fact that PEG microwells are poorly visible in the red image to detect and localize them. A well template was generated using a microwell image, and was matched against the R image to detect microwells. Given that R is a dead cell image (from 3×2 mosaic images) defined on a fixed digital grid D:

$$R = \left\{R_{ij} \,\middle|\, (i,j) \in D\right\}$$

$$[\text{Eq. 6}]$$

we defined z_w as the set of well centers in image R consisting of q_w well centers:

$$z_w = \left\{z_w^k \,\middle|\, k \in [1, q_w]\right\}$$

$$[\text{Eq. 7}]$$

One or a few microwells (I_W^n) in the image were selected by the user to generate the well template. Each microwell is selected by addressing the top left and the bottom right of it. We suggest selecting the microwells in an image taken of an empty array of microwells, however the well template can be generated by selecting microwells in an image taken from a cell-seeded array of microwells. Although microwell selection to generate a new template takes just a few seconds, we should point out that the procedure of microwell selection/generation was done once for the whole data set of 108 images (i.e., once a microwell template is generated, it can potentially be used for detection of microwells with the same shape). The well template (h_w) is generated by averaging the selected microwells:

$$h_w = \frac{1}{N} \sum_{n=1}^{N} I_W^n$$

$$[\text{Eq. 8}]$$

where h_w and I_W^n are the well template and the nth selected well respectively, represented as two-dimensional matrices. The convolution operation can be used for template matching where a symmetric kernel is used, therefore for an asymmetric kernel, the convolution kernel must be flipped and then be convolved with the image to generate the correlation map. As a symmetric kernel remains unchanged by flipping and we want to have a general method to be applicable to both symmetric and asymmetric kernels, i.e., both symmetric and asymmetric microwells, the generated well template is flipped (h_w^f) and then is convolved with the red image R to generate a correlation map:

$$H_w = R * h_w^f$$

$$[\text{Eq. 9}]$$

The well correlation map obtained by applying the well template is depicted in Figure 3B, part (*ii*). The brighter pixels in the correlation map show the highly correlated points which are more likely to be the well centers. To locate the well centers and remove the unlikely well centers, we find the local maxima in the well correlation map

$$L_w = l\left(H_w, W_w\right)$$

$$[\text{Eq. 10}]$$

where l is a function to locate the local maxima, L_w is the located local maxima in image R and W_w is the window size to be locally searched for the local maxima.
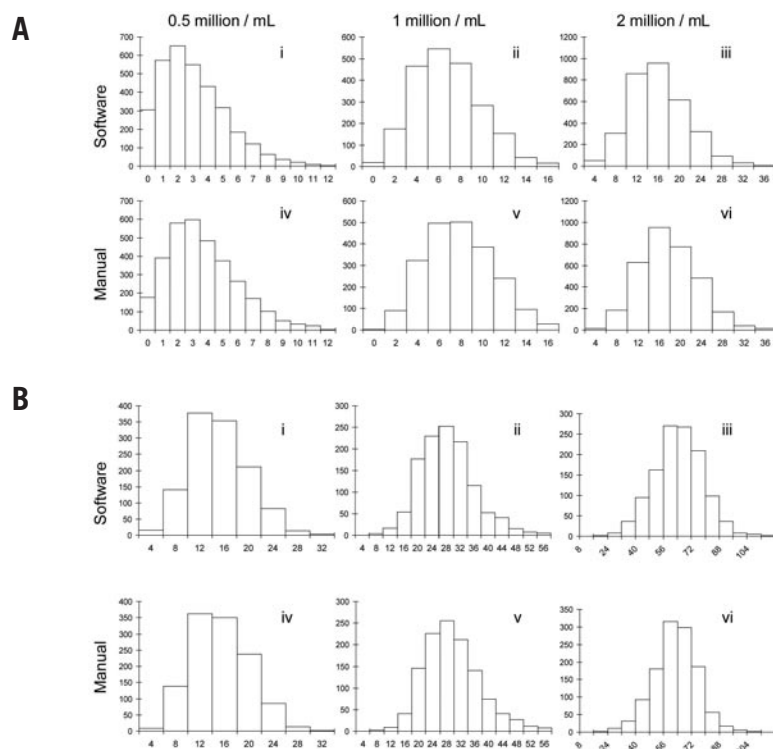
A

B

Figure 4. Frequency plots of the number of cells per well at 3 seeding concentrations. (A) The number of cells per well in 200-µm microwells. Parts (*i*)–(*iii*), software counting results; parts (*iv*)–(*vi*), manual counting results. (B) The number of cells per well in 400-µm microwells. Parts (*i*)–(*iii*), software counting results; parts (*iv*)–(*vi*), manual counting results. Cells per well values were plotted for the recurring counts against the respective cell numbers per well. The manual counting results were published earlier (18). **[Q17]**

The well center map is finally generated by thresholding the well local maxima map

$$Z_w = T\left(L_w, \tau_w\right)$$

[Eq. 11]

where T is a thresholding function to return a thresholded set Z_w containing those well local maxima which their values are greater than the threshold value τ_w. Localized well centers along with the template well diameter are used to generate a microwell map as depicted in Figure 3B, part (*iii*). The threshold is selected by minimizing the number of misdetections and false alarms; for a different data set, the user might need to set the threshold and visually inspect the result (to minimize misdetections and false alarms) in order to fine tune the threshold.

The live and dead cells encircled in each microwell are counted using the coordinates of the microwell center and microwell diameter. The red image was used to detect both the dead cells and microwells, while well boundary responded strongly to the cell template and resulted in significant number of false dead cell detections. To

overcome this problem, we considered a slightly smaller diameter with regard to the detected well center coordinates to encompass and count dead cells. As a result, once the well center coordinates were detected, the well diameter was used to encircle live cells in the green image, and a slightly smaller diameter was used to encircle dead cells in the red image.

Results

The proposed algorithm was developed in Matlab (The MathWorks, Natick, MA, USA) and used for microwell cell counting in array images. To test the performance, the automated cell counting was compared with manual cell counting reported previously (18). In the present version of the software, the predefined cell and well templates were used as correlation kernels, however, in the future work, we plan to enable the user to design new templates based on the cell type and well shape.

To start software cell counting, a fluorescent image is selected and loaded into the program. Figure 3B, part (*i*) shows a 3 × 3 microwell array cropped from the original fluorescent image. The microwell

correlation map, along with the live- and dead-cell correlation maps, are depicted in Figures 3B part (*ii*), 3A part (*i*), and 3A part (*iv*), respectively. The microwell centers are localized by thresholding the microwell local maxima map. As shown in Figure 3B, part (*iii*), the diameter of the detected microwells is set to be equal to that of the microwell template. The located live and dead cell centers are depicted in Figure 3A part (*ii*) and part (*v*), respectively while the located cell centers superimposed on the original green and red images are shown with gray level shadows in Figure 3A part (*iii*) and part (*vi*). Figure 3C shows the automated microwell cell counting result reported by the software for each microwell on the original fluorescent image of 11 × 17 microwells, where the total number of wells and cells are recorded on the bottom left of the image. As it is depicted in Figure 3, the microwells are precisely detected, both live and dead cells inside each microwell are counted, and the cell number per well is conveniently recorded on top of each microwell. In addition, the counts are also recorded by the software in a separate Microsoft Excel spread sheet for further studies.

To compare the automated counting results with the manual ones, all 108 images similar to the one shown in Figure 3C consisting of 22,000 microwells, and more than 500,000 cells were automatically counted using the software. As depicted in Figure 4, the histograms representing manual and software counting are almost identical, which shows the two counting results are analogous to each other. Figure 5 illustrates the average cell counts obtained by the two methods. As shown in Figure 5A part (*i*) and 5B part (*i*), the automated counting performs consistently and its outcome is similar to that of manual counting. Automatic cell counting takes <25 s in average to process an image with 1200 × 1600 resolution containing 250 microwells (with diameter of 200 microns) on a typical 1.6 GHz processor. The process time consists of the time fractions spent on well detection, live- and dead-cell detections, cell counting, and result reporting. The process is much faster than manual counting, can be applied in batch mode and overnight, and its precision is consistent over time (in contrast with the manual counting in which the counting precision might be decreased over time) **[Q8]**.

The mean cell counts in 200-µm wells were 5, 10, and 15 [Figure 5A, part (*i*)] while the absolute counting differences were 0.5, 1, and 2—equal to 10%, 10%, and 13.3%, respectively [Figure 5A, part (*ii*)]. The mean cell counts in 400-µm wells were
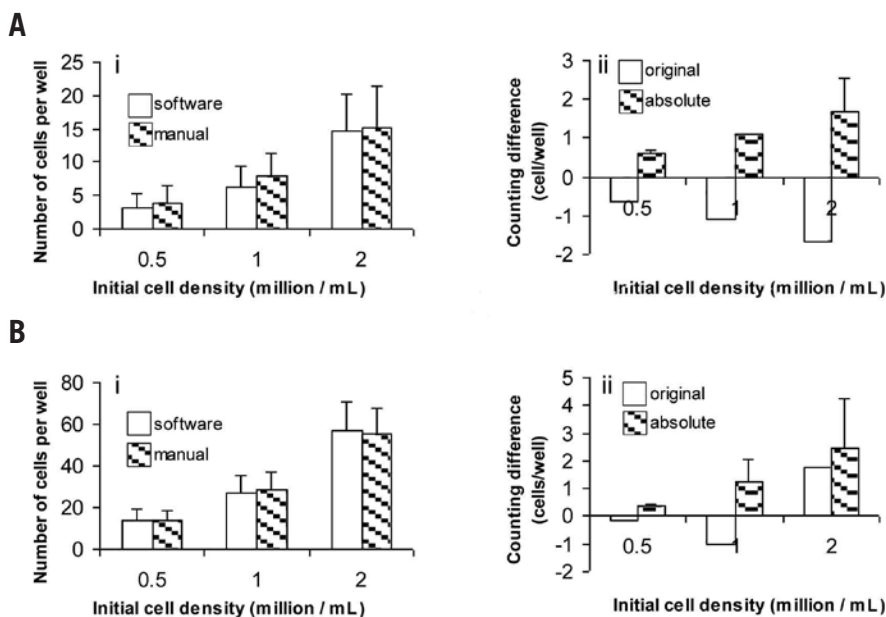
A

B

Figure 5. Software and manual counting comparisons for the number of cells per well. (A) 200-μm diameter microwells. (B) 400-μm diameter microwells. The cell number per well counts from software and manual counting methods are shown in panel A, part (*i*) and panel B, part (*i*), at 3 initial seeding concentrations. The differences of the counting were shown in panel A, part (*ii*) and panel B, part (*ii*), respectively, where the averages were calculated either by subtracting manual counts from software counts (original), or by subtracting manual counts from software counts the absolute and taking the average of their absolute values (absolute).**[Q18]**

15, 30, and 60 [Figure 5B, part (*i*)], while the absolute counting differences between the manual and automated counting were 0.5, 1, and 2—equal to 3.33%, 3.33%, and 3.33% respectively [Figure 5B, part (*ii*)].

Overall, the counting difference between the two methods ranged 0.5–2 cells/well. The proposed method performed robustly; however, as a typical pattern recognition problem, there were some misdetections in the counting results. To compare the counting methods, two differences are defined. The original difference is the average cell difference per well, which is obtained by summing up the automatic-manual counting differences for all wells and dividing the sum by the number of wells. In contrast, the absolute difference is computed by summing up the absolute automatic-manual counting differences for all wells and dividing the sum by the number of wells (Figure 5). Two possible sources for cell counting differences are as follows. First; manual cell counting results—though considered accurate—are subjective, may vary from person to person, and are prone to error **[Q9]**. Therefore, we used the term 'cell counting difference', (i.e., the difference between the two methods), in place of 'cell counting error.' Second; the red image is used for both dead-cell counting and well detection by applying cell and well templates respectively. Since

well boundary responds strongly to the cell template and causes a significant number of false detections, a slightly smaller well diameter has been used, which does omit dead cells that are located close or attached to the well boundary **[Q10]**.

It can be seen in Figure 4 that the cell counting difference is higher (10–13.3%) for 200-μm wells with 0.5–2 million cells/mL concentrations where the average number of seeded cells per well is low (5–15). In such cases, the effect of missing dead cells (considering smaller well diameter to encircle and count dead cells as it was mentioned earlier) in comparison with the average number of seeded cells was significant. Increasing the well diameter and cell concentration increases the precision of automatic cell counting (3.33%); the the influence of missing dead cells in comparison with the average number of seeded cells was insignificant.

Moreover, we compared the proposed Arraycount method with ImageJ. We wrote a plug-in for ImageJ using the ImageJ macro language. The macro can be installed in and used with ImageJ (version 1.41o). The major differences between Arraycount and the ImageJ macro be summarized as following. The ImageJ macro allows semi-automatic cell counting, but it is not capable of automatic well detection. Using the ImageJ plug-in, the user must

provide prior information such as the number of microwells in a matrix format (i.e., the number of rows and the number of columns). Moreover the user must provide the coordinates of three microwells including the top left, the top right, and the bottom left by drawing them. In this way, ImageJ plugin merely calculates the well coordinates based on information that is introduced by the user. In contrast, Arraycount is based on pattern recognition and image processing techniques for automatic detection of microwells, and does not need input information such as the number of microwells and their coordinates. Arraycount can also be used in batch mode (by writing a simple MatLab script), which allows continuous cell counting in many images, without user interference. Contrastly, in ImageJ, the user has to do the counting image by image. Overall, the ImageJ plug-in is adequate for small numbers of array images, while Arraycount is useful for large amounts of data in high-throughput screening **[Q11]**.

Discussion

This study establishes an approach for automatic cell counting in microarray format. The proposed method can be used to automatically recognize the location of each microwell on the microarray and then give the cell counts for each microwell in a timely fashion. It takes <0.1 s to detect a well and count its seeded cells. The proposed method, in ist current stage, is capable of localizing the specific microwells and cell type that have been used in our experiments; however, with reasonable efforts it can be adapted to count other cell types seeded in microwells with arbitrary shapes. In our experiments, the cells were fluorescent and the images were taken immediately after cell seeding, so the shape of the cells were shown to be round and uniform across the microwells; thus, it should be stressed that the proposed algorithm is efficient and accurate for counting cells where such conditions (roundness, uniformity) are maintained. It can potentially be used for stem cell research, but it has not been tested for counting cells in stem cell aggregates **[Q12]**. In the experiments that involve cell aggregates, in conditions where neighboring cells significantly overlap with each other, or in conditions where cell morphology may change, the cell counting is prone to error and it may not be desirable to use this method **[Q13]**.

In the proposed algorithm we assumed that cells are fluorescent, so in situations where the user needs to distinguish

features across cells such as antibody-stained microwells, it is not desirable to use the same fluorescence range, otherwise the results will prone to error. Also, in cases where the red stain spills outside of the microwells, the well detection would not be accurate due to the occlusion of well boundaries with the red stain in the red image.

Moreover, we assume uniform spatial illumination during imaging that sometimes may not be maintained. In such cases for precise cell counting and well detection, background estimation/subtraction must be applied in advance. Our future work focuses on employing the machine learning techniques to select or generate the appropriate cell and well templates using a template library.

Acknowledgments

References

1. **Kang, L., B.G. Chung, R. Langer, and A. Khademhosseini.** 2008. Microfluidics for drug discovery and development: from target selection to product lifecycle management. Drug Discov. Today *13*:1-13.

2. **Khademhosseini, A., R. Langer, J. Borenstein, and J.P. Vacanti.** 2006. Microscale technologies for tissue engineering and biology. Proc. Natl. Acad. Sci. USA *103*:2480-2487.

3. **Chin, V.I., P. Taupin, S. Sanga, J. Scheel, F.H. Gage, and S.N. Bhatia.** 2004. Microfabricated platform for studying stem cell fates. Biotechnol. Bioeng. *88*:399-415.

4. **Choi, I., Y.I. Yang, Y.J. Kim, Y. Kim, J.S. Hahn, K. Choi, and J. Yi.** 2008. Directed positioning of single cells in microwells fabricated by scanning probe lithography and wet etching methods. Langmuir *24*:2597-2602.

5. **Meek, C.C. and P. Pantano.** 2001. Spatial confinement of avidin domains in microwell arrays. Lab Chip *1*:158-163.

6. **Tokimitsu, Y., H. Kishi, S. Kondo, R. Honda, K. Tajiri, K. Motoki, T. Ozawa, S. Kadowaki, et al.** 2007. Single lymphocyte analysis with a microwell array chip. Cytometry A *71*:1003-1010.

7. **Karp, J.M., J. Yeh, G. Eng, J. Fukuda, J. Blumling, K.Y. Suh, J. Cheng, A. Mahdavi, et al.** 2007. Controlling size, shape and homogeneity of embryoid bodies using poly(ethylene glycol) microwells. Lab Chip *7*:786-794.

8. **Moeller, H.C., M.K. Mian, S. Shrivastava, B.G. Chung, and A. Khademhosseini.** 2008. A microwell array system for stem cell culture. Biomaterials *29*:752-763.

9. **Cordey, M., M. Limacher, S. Kobel, V. Taylor, and M.P. Lutolf.** 2008. Enhancing the reliability and throughput of neurosphere culture on hydrogel microwell arrays. Stem Cells *26*:2586-2594.

10. **Hsu, W., L.R. Long, and S. Antani.** 2007. SPIRS: a framework for content-based image retrieval from large biomedical databases. Stud. Health Technol. Inform. *129*:188-192.

11. **Karacali, B., A.P. Vamvakidou, and A. Tozeren.** 2007. Automated recognition of cell phenotypes in histology images based on membrane- and nuclei-targeting biomarkers. BMC Med. Imaging *7*:7.

12. **Lomenie, N., F. Richard, E. Dusch, and D. Segretain.** 2006. An automatic system for the analysis of intercellular communication and early carcinogenesis. Cell. Mol. Biol. (Noisy-le-grand) *52*:32-37.

13. **Selinummi, J., J. Seppala, O. Yli-Harja, and J.A. Puhakka.** 2005. Software for quantification of labeled bacteria from digital microscope images by automated image analysis. BioTechniques *39*:859-863.

14. **Lamprecht, M.R., D.M. Sabatini, and A.E. Carpenter.** 2007. CellProfiler: free, versatile software for automated biological image analysis. Biotechniques *42*:71-75.

15. **Bewes, J.M., N. Suchowerska, and D.R. McKenzie.** 2008. Automated cell colony counting and analysis using the circular Hough image transform algorithm (CHiTA). Phys. Med. Biol. *53*:5991-6008.

16. **Dahle, J., M. Kakar, H.B. Steen, and O. Kaalhus.** 2004. Automated counting of mammalian cell colonies by means of a flat bed scanner and image processing. Cytometry A *60*:182-188.

17. **Peng, H.** 2008. Bioimage informatics: a new area of engineering biology. Bioinformatics *24*:1827-1836.

18. **Kang, L., M.J. Hancock, M.D. Brigham, and A. Khademhosseini.** Cell confinement in patterned nanoliter droplets in a microwell array by wiping. J. Biomed. Mater. Res. A. (In press).

19. **Parida, S.K. and B.K. Mishra.** 1998. Adsorption of styryl pyridinium dyes on polyethylene-glycol-treated silica. Colloids Surf. A: Physicochem. Eng. Asp. *134*:249-255.

Address correspondence to Ali Khademhosseini, 65 Landsdowne Street, Room 252, Cambridge, MA, 02139, USA. email: alik@mit.edu